

Optomechanical crystal nanobeam cavity with high optomechanical coupling rate

This content has been downloaded from IOPscience. Please scroll down to see the full text.

2015 J. Opt. 17 045001

(<http://iopscience.iop.org/2040-8986/17/4/045001>)

View [the table of contents for this issue](#), or go to the [journal homepage](#) for more

Download details:

IP Address: 166.111.65.62

This content was downloaded on 20/03/2015 at 05:58

Please note that [terms and conditions apply](#).

Optomechanical crystal nanobeam cavity with high optomechanical coupling rate

Yongzhuo Li, Kaiyu Cui, Xue Feng, Yidong Huang, Zhilei Huang, Fang Liu and Wei Zhang

Department of Electronic Engineering, Tsinghua National Laboratory for Information Science and Technology, Tsinghua University, Beijing 100084, People's Republic of China

E-mail: kaiyucui@tsinghua.edu.cn

Received 3 September 2014, revised 2 December 2014

Accepted for publication 21 January 2015

Published 26 February 2015



CrossMark

Abstract

An optomechanical crystal nanobeam cavity, only by increasing the radius of air holes in the defect region, is proposed and optimized for a high optomechanical coupling rate. In our proposed cavity, the photonic and phononic defect modes are simultaneously confined by each corresponding bandgap, and the overlap of the optical and mechanical modes can be improved simply by adjusting the radius of the air holes. Accordingly, an optomechanical coupling rate (g) as high as 1.16 MHz is obtained, which is the highest coupling rate among the reported optomechanical crystal cavities. What's more, the proposed cavity also exhibits a high mechanical frequency of 4.01 GHz and a small effective mass of 85 fg for the fundamental mechanical mode.

Keywords: acousto-optical devices, optomechanics, photonic crystals, optical resonators

(Some figures may appear in colour only in the online journal)

1. Introduction

Recently, optical forces, including the radiation pressure forces [1, 2] and the optical gradient forces [3, 4], have been used to control nanoparticles or manipulate nanoscale waveguides and resonators. Among them, cavity optomechanics [5–8], exploring the interaction of optical and mechanical modes in various optical cavities, have developed quickly in a wide range of applications, including laser cooling of the mechanical motion to its quantum ground state [9–11], photon–phonon translation [12], sensing [13, 14], and so on, because the radiation pressure forces acting on the micro/nanoscale mechanical objects can be enhanced by the high optical field intensity in the cavities. Thanks to the development of nanofabrication techniques, optomechanical resonators such as vibrating microtoroids [15], vertically coupled disk resonators [16], and laterally coupled ladder photonic crystal cavities [17, 18] have been studied recently. For an optomechanical system, the coupling between mechanical and optical modes is the key point, and a high coupling rate is necessary for various applications based on cavity optomechanics. In order to enhance the coupling between mechanical and optical modes, various optomechanical

structures have been reported. A typical one is optomechanical crystals [19] or phoxonic crystals [20, 21], which can simultaneously form phononic and photonic crystal bandgaps by their periodic structures. Introducing defects into the one-dimensional optomechanical crystals forms optomechanical crystal nanobeam cavities, where both photons and phonons can be confined in a very small region around the cavity center. A high optomechanical coupling rate (g) of 910 kHz was realized in this kind of nanobeam cavity [9] by a rather complicated design of the nanobeam structure with irregular elliptical air holes. The optomechanical coupling rate is much higher than that of other kinds of optomechanical cavities [4, 22, 23], and, as a result, mechanical motion can be cooled down to its quantum ground state at a bath temperature of 20 K.

In order to further improve the optomechanical coupling rate with simple and regular patterns, we propose an optomechanical crystal nanobeam cavity only by increasing the radius of air holes in the defect region. The high coupling rate can be achieved by changing the ratio of radius and period (r_0/a) to improve the overlap of optical field and mechanical field and confine them in a smaller region. The simulation results show that an optomechanical coupling rate as high as

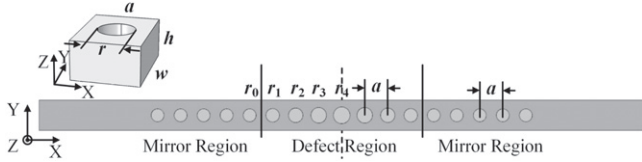


Figure 1. The 2D schematic of the proposed optomechanical crystal nanobeam cavity and a 3D unit cell.

1.16 MHz can be obtained, which is the highest coupling rate for the reported optomechanical crystal cavities. The remarkable thing is, the proposed nanobeam cavity also exhibits a high mechanical frequency (ω_m) of 4.01 GHz with an effective mass (m_{eff}) of only 85 fg.

2. Cavity designs

The two-dimensional (2D) schematic of the proposed optomechanical crystal nanobeam cavity and a three-dimensional (3D) unit cell are shown in figure 1, which consists of a single row of holes embedded in a 515 nm-wide (w) ridge waveguide. This structure is formed in the device layer of a silicon-on-insulator (SOI) chip with a refractive index of 3.48. The buried oxide in the SOI chip is removed to form an air-bridge structure. The thickness of the device layer is 220 nm, denoted by h . The optomechanical crystal nanobeam cavity consists of two mirror regions and one defect region. In the mirror regions, the lattice constant (a) and radius (r_0) of the periodic air holes are 402 nm and 105.7 nm, respectively, while the radius of the air holes in the defect region gradually increases from r_0 to r_4 by a step of $0.16 r_0$, as shown in figure 1.

The principle for our design can be explained by the photonic and phononic bands of the optomechanical crystal with the given periodic structures. The photonic band diagram of TE modes is calculated by the plane-wave expansion method with two different r/a of 0.263(105.7 nm/402 nm) and 0.342(137.5 nm/402 nm), which is shown in figure 2(a). The light line (blue line) is the dispersion curve for light in vacuum and divides the diagram into two regions. The radiative modes lie above the light line in the gray region, and the guided modes lie in the region below the light line. It can

be seen that the frequency of the guided optical mode increases with a larger ratio of r/a . Therefore, by introducing a defect with holes of a larger radius in the periodic structure, there will be a defect mode in the bandgap (dark gray region) when k_x is chosen at the X symmetric point, where k_x is the wave vector along the x direction.

Based on the same principle, the phononic defect mode can also be formed in the same structure, which is presented in the phononic band diagram of figure 2(b). Here, the phononic bands are calculated by the finite element method (FEM) with periodic boundary conditions applied in the x direction and free boundary conditions in the y and z directions [17, 19]. In the calculation, the density of silicon is set at $\rho = 2330 \text{ kg m}^{-3}$, and the full anisotropic elasticity matrix is used, where $(C_{11}, C_{12}, C_{44}) = (166, 64, 80)$ GPa. When the ratio of r/a is increased to 0.342, the phononic frequency is decreased. As a result, there is a defect mode in the bandgap (dark gray region) of the periodic structure with $r/a = 0.263$ when k_x is chosen at the Γ symmetric point, and the phononic bandgap is between 3.9–5.3 GHz. Thus, taking into account the generation of photonic and phononic defect modes, we can form the photonic and phononic defect modes in each bandgap simultaneously by only increasing the radius of the air holes in the defect region of the proposed nanobeam cavity.

3. Mechanical modes of the nanobeam cavity

The mechanical properties for our proposed structure are mainly evaluated by three figures of merit, including the mechanical eigenfrequency of the nanobeam cavity, the mechanical quality factor (Q_m), and the effective mass. The mechanical eigenfrequency is the resonant frequency of phonon in the nanobeam cavity. The mechanical quality factor describes the loss of mechanical energy for the nanobeam cavity. The effective mass is proportional to the volume of the mechanical mode, which represents the effective localization of the mechanical mode within a material of constant mass density and elastic moduli. In our investigation, the mechanical properties of the nanobeam cavity are numerically simulated via the 3D FEM, where fixed boundary conditions are applied at both ends of the nanobeam cavity

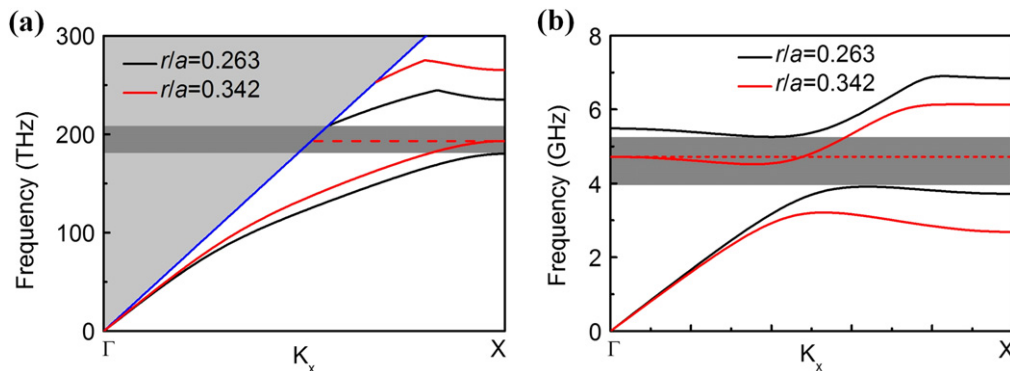


Figure 2. (a) The optical band structure for propagation along the x -axis in the unit cell with different ratios of r/a ; (b) the mechanical band structure for propagation along the x -axis in the unit cell with different ratios of r/a .

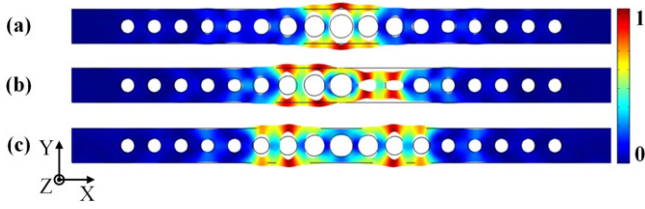


Figure 3. (a)–(c) The displacement fields of the fundamental, second-order, and third-order mechanical modes of the nanobeam cavity.

along the x direction, and free boundary conditions are applied in the y and z directions.

The eigenfrequencies of the fundamental, second-order, and third-order mechanical modes of the nanobeam cavity are 4.01 GHz, 4.34 GHz, and 4.7 GHz, respectively, and the displacement fields ($Q(r)$) of these modes are shown in figures 3(a)–(c). The mechanical frequency of 4.01 GHz for the fundamental mechanical mode is much higher than that of several hundred MHz in [7, 8]. The radius of the air holes in the defect region gradually increases by a step of $0.16r_0$ from r_0 to r_4 , while the other parameters are the same as those mentioned above.

The mechanical quality factor is affected by various intrinsic and extrinsic mechanisms, e.g., the Akhieser/Landau–Rumer mechanism, clamping, thermoelastic damping, defect motion, and air damping, etc [24]. Among these, the Akhieser/Landau–Rumer mechanism, clamping loss, and thermoelastic damping are the dominant loss mechanisms for the nanobeam cavities. Therefore, Q_m is given by

$$\frac{1}{Q_m} = \frac{1}{Q_{m_AL}} + \frac{1}{Q_{m_TE}} + \frac{1}{Q_{m_CL}}. \quad (1)$$

The Akhieser/Landau–Rumer losses are mainly from the interaction between phonons and thermal phonons, which describe the absorption of phonons by the material. The Akhieser mechanism is valid for an acoustic wavelength much larger than the mean free path of the thermal phonons. On the other hand, the Landau–Rumer mechanism is valid for an acoustic wavelength less than the mean free path of the thermal phonons. The absorption coefficients for the above mechanism are given by [25]

$$\alpha = \begin{cases} \frac{\gamma^2 \omega_m^2 T \kappa}{\rho c_s^5}, & \text{(Akhieser)} \\ \frac{\pi \gamma^2 \omega_m C_V T}{4 \rho c_s^3}, & \text{(Landau–Rumer)}, \end{cases} \quad (2)$$

where γ is the Grüneisen parameter, T is the temperature, κ is the thermal conductivity, c_s is the acoustic velocity, and C_V is the volumetric heat capacity. Q_{m_AL} can be estimated from the equation as $Q_{m_AL} = \omega_m / 2\alpha c_s$. The calculation results show that Q_{m_AL} of the mechanical fundamental mode is about 3.3×10^4 at the temperature of 300 K, where the equation derived from the Akhieser mechanism is used. When the temperature is 20 K, the calculated Q_{m_AL} can reach

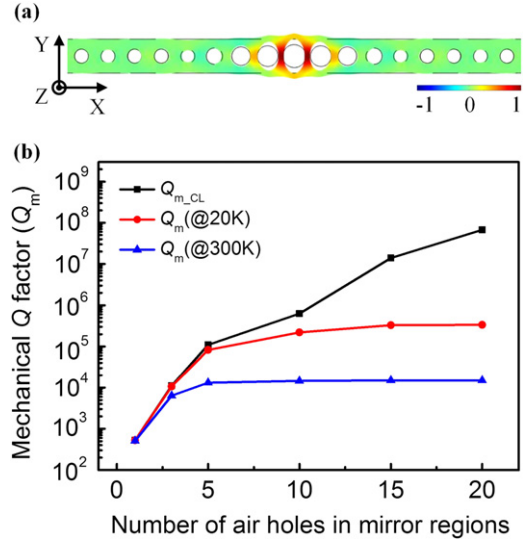


Figure 4. (a) The normalized thermal profile for the 4.01 GHz fundamental mechanical mode at 300 K; (b) the curves of Q_{m_CL} and Q_m versus different numbers of air holes in the mirror regions.

1.2×10^6 , where the equation derived from the Landau–Rumer mechanism is used.

Thermoelastic damping, as an intrinsic material damping, arises from the coupling of the displacement field to a temperature field. The normalized thermal profile for the 4.01 GHz fundamental mechanical mode at 300 K is simulated and shown in figure 4(a). The corresponding mechanical quality factor considering the thermoelastic damping effect (Q_{m_TE}) is around 2.72×10^4 , while Q_{m_TE} is decided by the temperature. With the temperature decreased, Q_{m_TE} increases and reaches 4.7×10^5 at 20 K.

Clamping loss is attributed to acoustic energy leaking into the substrate via the clamping points of the nanobeam. The corresponding mechanical quality factor regarding clamping loss, denoted as Q_{m_CL} , can be obtained from the complex eigenfrequency, which is calculated by adding perfectly matched layers at both ends of the nanobeam as an efficient impedance-matched nonphysical material for absorbing the radiating elastic waves without reflection. The mirror regions of the nanobeam can effectively reflect the elastic waves, so it's possible to reduce the clamping loss simply by increasing the number of air holes in the mirror regions. Figure 4(b) shows the curves of Q_{m_CL} and Q_m versus different numbers of air holes. It can be seen that with the number of air holes in the mirror regions increasing from 1 to 20, Q_{m_CL} rises from 10^2 to 10^7 . As a result, Q_m is greater than 1.5×10^4 when the number of air holes in the mirror regions is more than five at 300 K. When the temperature is at 20 K, Q_m can be greater than 3.4×10^5 with more than 15 air holes in mirror regions. In addition, a full phononic shield, proposed in [9, 26], can also be used for our cavity to further improve the mechanical quality factor.

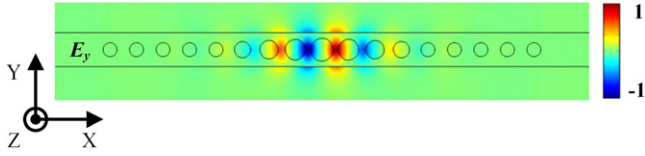


Figure 5. Mode profile of the electric field component E_y for the nanobeam cavity.

Finally, the effective mass is computed from

$$m_{\text{eff}} = \int \rho \left(|Q(r)|^2 / |Q(r)|_{\text{max}}^2 \right) dV, \quad (3)$$

where $|Q(r)|_{\text{max}}$ is the maximum displacement [27]. The effective mass of the fundamental, second-order, and third-order mechanical modes are computed to be 85 fg, 167 fg, and 170 fg, respectively. Compared with other optomechanical systems, like doubly clamped beams ($m_{\text{eff}} = 190 \mu\text{g}$) [28], mirotoroids ($m_{\text{eff}} = 10 \text{ ng}$) [15], two vertically stacked ring cavities ($m_{\text{eff}} = 85 \text{ pg}$) [16], and 2D photonic crystal cavities ($m_{\text{eff}} = 200 \text{ fg}$) [7], the effective mass of our proposed structure is very small.

4. Optical mode of the nanobeam cavity

In our proposed structure, the confinement for the optical cavity mode in the x direction is mainly governed by the distributed Bragg reflection of the air holes. As shown in figure 2(a), by increasing the radius of the air hole in the center of nanobeam cavity, there will be a defect mode in the photonic bandgap, which can be confined in the defect region. The confinement in the y and z directions, on the other hand, is due to total internal reflection [29]. The optical properties of the nanobeam cavity are studied by using the 3D finite-difference time-domain method. Figure 5 shows the calculated electric field component E_y distribution of the TE mode at a frequency of 200 THz.

5. Optomechanical coupling rate

In the optomechanical nanobeam cavity, the optical and mechanical modes are mutually coupled. The optical force generated by the injected photons inside the nanobeam cavity makes a slight structural deformation around the center of the cavity. In turn, the optical field is modified by the moving dielectric boundary [30] and the change of refractive index caused by the strain field, which is called the photo-elastic effect [31]. To quantify the interaction between photons and phonons, the optomechanical coupling rate is defined as

$$g = x_{\text{zpf}} d\omega_o / d\alpha, \quad (4)$$

where ω_o is the angular frequency of the optical mode and α is the amplitude of the mechanical displacement field [26]. $d\omega_o / d\alpha$ demonstrates the strength of optomechanical transductions and is calculated by first-order electromagnetic

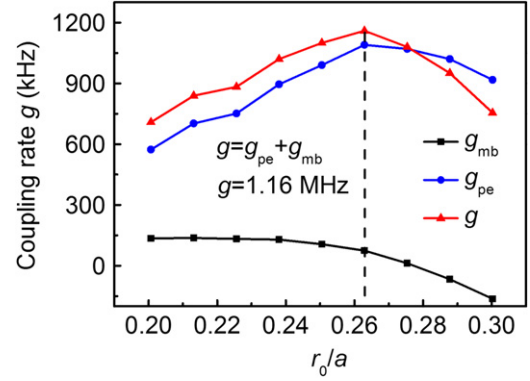


Figure 6. Optomechanical coupling rates versus different r_0/a in the proposed optomechanical crystal nanobeam cavities.

perturbation theory. x_{zpf} is the zero-point motion of the mechanical mode and expressed as $x_{\text{zpf}} = \sqrt{\hbar / 2m_{\text{eff}}\omega_m}$; here ω_m is the angular mechanical frequency. Given the contribution of the moving dielectric boundary and the photo-elastic effect, the total optomechanical coupling rate can be approximately divided into two parts.

$$g = g_{\text{mb}} + g_{\text{pe}} = \left(\left. \frac{d\omega_o}{d\alpha} \right|_{\text{mb}} + \left. \frac{d\omega_o}{d\alpha} \right|_{\text{pe}} \right) x_{\text{zpf}} \quad (5)$$

g_{mb} is calculated by using the perturbation theory for Maxwell's equations with shifting boundaries and expressed as [32]

$$\left. \frac{d\omega_o}{d\alpha} \right|_{\text{mb}} = -\frac{\omega_o}{2} \frac{\oint (\mathbf{q} \cdot \hat{\mathbf{n}}) (\Delta\epsilon E_{\parallel}^2 - \Delta\epsilon^{-1} D_{\perp}^2) ds}{\int \epsilon |E|^2 dV}, \quad (6)$$

where \mathbf{q} is the normalized displacement field, $\hat{\mathbf{n}}$ is the unit normal vector at the surface of the unperturbed cavity; E and D are the unperturbed electric field and the electric displacement field, respectively; the subscripts \parallel and \perp denote the field components parallel and perpendicular to the boundary surface, respectively; $\Delta\epsilon$ is defined as $\epsilon_{\text{si}} - \epsilon_{\text{air}}$; and $\Delta\epsilon^{-1}$ is defined as $\epsilon_{\text{si}}^{-1} - \epsilon_{\text{air}}^{-1}$ [30].

The contribution of the photo-elastic effect is from the change of the refractive index caused by the variation in strain. Based on the same displacement field, $d\epsilon / d\alpha$ is given by [33]

$$\frac{d\epsilon}{d\alpha} = -\epsilon \left(\frac{\mathbf{pS}}{\epsilon_0} \right) \epsilon, \quad (7)$$

where \mathbf{p} is the rank-four photo-elastic tensor and \mathbf{S} is the strain tensor. The photo-elastic coefficients for silicon are $(p_{11}, p_{12}, p_{44}) = (-0.094, 0.017, -0.051)$ [31]. Based on these, the full first-order correction attributed to the photo-elastic

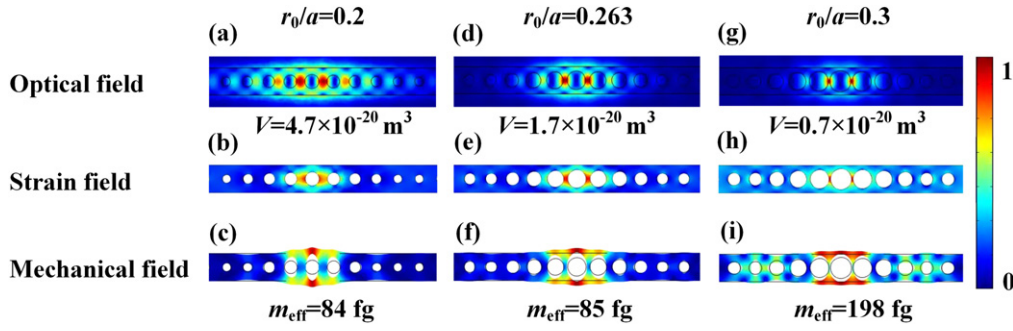


Figure 7. (a)–(c) Optical, strain, and mechanical fields of the nanobeam cavity with $r_0/a=0.2$; (d), (e) Optical, strain, and mechanical fields of the nanobeam cavity with $r_0/a=0.263$; (g)–(i) Optical, strain, and mechanical fields of the nanobeam cavity with $r_0/a=0.3$.

effect is [26]

$$\begin{aligned} \frac{d\omega_o}{d\alpha} \Big|_{pe} &= \frac{\omega_o \epsilon_0 n^4}{2} \int \left[2 \operatorname{Re} \{ E_x^* E_y \} p_{44} S_{xy} + 2 \operatorname{Re} \{ E_x^* E_z \} \right. \\ &\quad \times p_{44} S_{xz} + 2 \operatorname{Re} \{ E_y^* E_z \} p_{44} S_{yz} \left. \right] + |E_x|^2 \\ &\quad \times \left(p_{11} S_{xx} + p_{12} (S_{yy} + S_{zz}) \right) + |E_y|^2 \\ &\quad \times \left(p_{11} S_{yy} + p_{12} (S_{xx} + S_{zz}) \right) + |E_z|^2 \\ &\quad \times \left(p_{11} S_{zz} + p_{12} (S_{xx} + S_{yy}) \right) dV / \int \epsilon |E|^2 dV. \quad (8) \end{aligned}$$

Based on the expressions (5)–(8), the optomechanical coupling between the optical mode and the fundamental, second-order, and third-order mechanical modes are calculated. The coupling rates are 1160 kHz, 0.4 kHz, and 299 kHz, respectively. From the results, we can see that the coupling between the optical mode and the fundamental mechanical mode is higher than the coupling between the optical mode and high-order mechanical modes. As a result, we mainly investigate the coupling characteristic between the optical mode and the fundamental mechanical mode.

To investigate the influence of structural parameters on g_{mb} and g_{pe} , we calculate those with different r_0/a , as shown in figure 6. With r_0/a increasing from 0.2 to 0.263, g dramatically increases from 708 kHz to 1160 kHz. Then g decreases when $r_0/a > 0.263$. Actually, g is decided by the overlap of optical fields and mechanical fields, according to equations (6) and (8). From figure 6, it can be seen that the photo-elastic effect contributes more to the coupling rate under a fixed r_0/a . With r_0/a increased from 0.2 to 0.263, g_{pe} dramatically increases from 573 kHz to 1090 kHz. According to equation (8), g_{pe} is mainly decided by the overlap of optical and strain fields. Here, the strain field is the differential of the displacement field. As shown in figures 7(a)–(c), when $r_0/a=0.2$, the distribution of the optical field is larger than that of the strain field. The small overlap results in a low coupling rate, while with the increase of r_0/a , the mode volume (V) of the optical mode is reduced. As shown in figures 7(d)–(f), the optical field is confined in a small region, which is close to that of the strain field. Therefore, the high overlap of these fields improves the coupling rate. Then, when r_0/a is increased to 0.3, the overlap of the optical and strain fields

decreases, which results in the reduction of g_{pe} from 1090 kHz to 917 kHz. On the other hand, g_{mb} descends from 74 kHz to -163 kHz with r_0/a increased from 0.263 to 0.3. As a result, the optomechanical coupling rate reaches the maximum of 1.16 MHz at $r_0/a=0.263$, then decreases when $r_0/a > 0.263$. In our proposed structure, the high coupling rate can be achieved by changing r_0/a to improve the overlap between the optical field and the mechanical field and confine them in a small region.

The optomechanical coupling rate quantifies the interaction between a single photon and a single phonon. Thus, it will not be affected by the thermal environment. In addition, there is another parameter, named the optomechanical gain factor, to describe the interaction between the optical and mechanical modes, as seen in [34, 35]. The optomechanical gain factor is inversely proportional to the mechanical dissipation rate. So, it will be reduced by the mechanical loss from the thermal environment.

Recently, an optomechanical coupling rate of 148 kHz in a photonic crystal cavity has been measured in experiment [36, 37]. The experimental setup provides a feasible solution to determine the optomechanical parameters for the optomechanical systems. In the future, the optomechanical coupling rate of our proposed nanobeam cavity will be measured in experiment. Based on the high optomechanical coupling rate, further experiments can be envisioned, such as laser cooling of the nanobeam cavity to its ground state.

6. Conclusion

In this paper, an optomechanical crystal nanobeam cavity is proposed and optimized for a high optomechanical coupling rate. Only by adjusting the radius of the air holes, the proposed structure can simultaneously confine the photonic and phononic defect modes by each corresponding bandgap and improve the overlap of the optical and mechanical modes. As a result, an optomechanical coupling rate as high as 1.16 MHz is obtained, which is the highest coupling rate among the reported optomechanical crystal cavities. Moreover, the nanobeam cavity exhibits a high mechanical frequency of 4.01 GHz with a small effective mass of 85 fg.

Acknowledgments

This work was supported by the National Basic Research Program of China (No. 2011CBA00608, 2011CBA00303, 2011CB301803, and 2010CB327405), the National Natural Science Foundation of China (Grants No. 61307068, 61036010, 61036011, and 61321004). This project is partially funded by Tsinghua—Toshiba Energy and Environment Research Center. The authors would like to thank Mr Shichao Chen for his valuable discussions and helpful comments.

References

- [1] Carmon T, Rokhsari H, Yang L, Kippenberg T J and Vahala K J 2005 Temporal behavior of radiation-pressure-induced vibrations of an optical microcavity phonon mode *Phys. Rev. Lett.* **94** 223902
- [2] Rokhsari H, Kippenberg T J, Carmon T and Vahala K J 2006 Theoretical and experimental study of radiation pressure induced mechanical oscillations (parametric instability) in optical microcavities *IEEE Journal of Selected Topics in Quantum Electronics* **12** 96–107
- [3] Zhang X, Tomes M and Carmon T 2011 Precession optomechanics *Opt. Express* **19** 9066–73
- [4] Van Thourhout D and Roels J 2010 Optomechanical device actuation through the optical gradient force *Nat. Photonics* **4** 211–7
- [5] Aspelmeyer M, Kippenberg T J and Marquardt F 2013 Cavity optomechanics (arXiv:1303.0733)
- [6] Kippenberg T J and Vahala K J 2008 Cavity optomechanics: back-action at the mesoscale *Science* **321** 1172–6
- [7] Li Y, Zheng J J, Gao J, Shu J, Aras M S and Wong C W 2010 Design of dispersive optomechanical coupling and cooling in ultrahigh-Q/V slot-type photonic crystal cavities *Opt. Express* **18** 23844–56
- [8] Zheng J, Sun X, Li Y, Poot M, Dadgar A, Shi N N, Pernice W H P, Tang H X and Wong C W 2012 Femtogram dispersive L3-nanobeam optomechanical cavities design and experimental comparison *Opt. Express* **20** 26486–98
- [9] Chan J, Alegre T, Safavi-Naeini A H, Hill J T, Krause A, Groblacher S, Aspelmeyer M and Painter O 2011 Laser cooling of a nanomechanical oscillator into its quantum ground state *Nature* **478** 89–92
- [10] Rocheleau T, Ndukum T, Macklin C, Hertzberg J B, Clerk A A and Schwab K C 2010 Preparation and detection of a mechanical resonator near the ground state of motion *Nature* **463** 72–5
- [11] Teufel J D, Donner T, Li D L, Harlow J W, Allman M S, Cicak K, Sirois A J, Whittaker J D, Lehnert K W and Simmonds R W 2011 Sideband cooling of micromechanical motion to the quantum ground state *Nature* **475** 359–63
- [12] Safavi-Naeini A H, Alegre T, Chan J, Eichenfield M, Winger M, Lin Q, Hill J T, Chang D E and Painter O 2011 Electromagnetically induced transparency and slow light with optomechanics *Nature* **472** 69–73
- [13] Krause A G, Winger M, Blasius T D, Lin Q and Painter O 2012 A high-resolution microchip optomechanical accelerometer *Nat. Photonics* **6** 768–72
- [14] Deng Y, Liu F, Leseman Z C and Hossein-Zadeh M 2013 Thermo-optomechanical oscillator for sensing applications *Opt. Express* **21** 4653–64
- [15] Schliesser A, Riviere R, Anetsberger G, Arcizet O and Kippenberg T J 2008 Resolved-sideband cooling of a micromechanical oscillator *Nat. Phys.* **4** 415–9
- [16] Wiederhecker G S, Chen L, Gondarenko A and Lipson M 2009 Controlling photonic structures using optical forces *Nature* **462** 103–633
- [17] Eichenfield M, Camacho R, Chan J, Vahala K J and Painter O 2009 A picogram- and nanometre-scale photonic-crystal optomechanical cavity *Nature* **459** 550–79
- [18] Gong Y Y, Rundquist A, Majumdar A and Vuckovic J 2011 Low power resonant optical excitation of an optomechanical cavity *Opt. Express* **19** 1429–40
- [19] Eichenfield M, Chan J, Camacho R M, Vahala K J and Painter O 2009 Optomechanical crystals *Nature* **462** 78–82
- [20] Psarobas I E, Papanikolaou N, Stefanou N, Djafari-Rouhani B, Bonello B and Laude V 2010 Enhanced acousto-optic interactions in a one-dimensional phoxonic cavity *Phys. Rev. B* **82** 174303
- [21] Laude V, Beugnot J-C, Benchabane S, Pennec Y, Djafari-Rouhani B, Papanikolaou N, Escalante J M and Martinez A 2011 Simultaneous guidance of slow photons and slow acoustic phonons in silicon phoxonic crystal slabs *Opt. Express* **19** 9690–8
- [22] Povinelli M L, Johnson S G, Lončar M, Ibanescu M, Smythe E J, Capasso F and Joannopoulos J D 2005 High-Q enhancement of attractive and repulsive optical forces between coupled whispering-gallery-mode resonators *Opt. Express* **13** 8286–95
- [23] Anetsberger G, Arcizet O, Unterreithmeier Q P, Rivière R, Schliesser A, Weig E M, Kotthaus J P and Kippenberg T J 2009 Near-field cavity optomechanics with nanomechanical oscillators *Nature Phys.* **5** 909–14
- [24] Mohanty P, Harrington D A, Ekinici K L, Yang Y T, Murphy M J and Roukes M L 2002 Intrinsic dissipation in high-frequency micromechanical resonators *Phys. Rev. B* **66** 085416
- [25] Woodruff T O and Ehrenreich H 1961 Absorption of sound in insulators *Phys. Rev.* **123** 1553–9
- [26] Chan J, Safavi-Naeini A H, Hill J T, Meenehan S and Painter O 2012 Optimized optomechanical crystal cavity with acoustic radiation shield *Appl. Phys. Lett.* **101** 081115
- [27] Eichenfield M, Chan J, Safavi-Naeini A H, Vahala K J and Painter O 2009 Modeling dispersive coupling and losses of localized optical and mechanical modes in optomechanical crystals *Opt. Express* **17** 20078–98
- [28] Arcizet O, Cohadon P-F, Briant T, Pinard M and Heidmann A 2006 Radiation-pressure cooling and optomechanical instability of a micromirror *Nature* **444** 71–4
- [29] Li Y, Cui K, Feng X, Huang Y, Wang D, Huang Z and Zhang W 2013 Photonic crystal nanobeam cavity with stagger holes for ultrafast directly modulated nano light emitting diodes *IEEE Photonics Journal* **5** 4700306
- [30] Johnson S G, Ibanescu M, Skorobogatiy M A, Weisberg O, Joannopoulos J D and Fink Y 2002 Perturbation theory for Maxwell's equations with shifting material boundaries *Phys. Rev. E* **65** 066611
- [31] David K and Biegelsen 1974 Photoelastic tensor of silicon and the volume dependence of the average gap *Phys. Rev. Lett.* **32** 1196–9
- [32] Safavi-Naeini A H and Painter O 2010 Design of optomechanical cavities and waveguides on a simultaneous bandgap phononic-photonic crystal slab *Opt. Express* **18** 14926–43
- [33] Yariv A and Yeh P 1984 *Optical Waves in Crystals* (New York: Wiley)
- [34] Butsch A, Koehler J R, Noskov R E and Russell P S J 2014 CW-pumped single-pass frequency comb generation by resonant optomechanical nonlinearity in dual-nanoweb fiber *Optica* **1** 158–64
- [35] Butsch A, Kang M S, Euser T G, Koehler J R, Rammler S, Keding R and Russell P S J 2012 Optomechanical nonlinearity in dual-nanoweb structure suspended inside capillary fiber *Phys. Rev. Lett.* **109** 183904

- [36] Gavartin E, Braive R, Sagnes I, Arcizet O, Beveratos A, Kippenberg T J and Robert-Philip I 2011 Optomechanical coupling in a two dimensional photonic crystal defect cavity *Phys. Rev. Lett.* **106** 203902
- [37] Gorodetsky M L, Schliesser A, Anetsberger G, Deleglise S and Kippenberg T J 2010 Determination of the vacuum optomechanical coupling rate using frequency noise calibration *Opt. Express* **18** 23236–46